RSC Advances

PAPER

View Article Online
View Journal | View Issue

Cite this: *RSC Adv.*, 2024, **14**, 39890

Desorption of pharmaceutical hydrochlorides from transition metal oxide nanoparticles – investigation by capillary electrophoresis

Eman T. Elmorsi and Edward P. C. Lai *

The binding affinity of pharmaceutical hydrochlorides onto transition metal oxide nanoparticles (TMONPs) was investigated through a consecutive process of adsorption and desorption. Mexiletine (MEX) was chosen as a model pharmaceutical hydrochloride that bound onto TMONPs' surface through electrostatic interactions and coordination bonding. Response surface methodology was applied for their optimal separation by capillary electrophoresis to achieve accurate quantitation. Linear and quadratic regressions were applied to model peak resolution and migration times. The response surface methodology was next applied to investigate the maximum desorption percentages of mexiletine (MEX) from the surface of TiO_2 and Co_3O_4 nanoparticles. ANOVA indicated a positive correlation between the MEX desorption results with pH, metformin (MET) competitive desorption agent concentration, Na_2HPO_4 concentration (hence ionic strength), and $Na_2S_2O_5$ reducing agent concentration. The MEX desorption increased from TiO_2 (46 ± 1%) to Co_3O_4 (63 ± 1%), suggesting a stronger binding interaction between MEX and TiO_2 nanoparticles. TiO_2 exhibited the order of pH > [MET] > [Na_2HPO_4] > [$Na_2S_2O_5$]; Co_3O_4 exhibited the order [Na_2HPO_4] > pH > [MET] > [$Na_2S_2O_5$]. This novel finding demonstrates the potential of TMONPs for use as efficient adsorbents to remove pharmaceutical compounds that accidently enter environmental water sources, with feasible regeneration.

Received 2nd October 2024
Accepted 3rd December 2024

DOI: 10.1039/d4ra07081j

rsc.li/rsc-advances

1. Introduction

The widespread use of pharmaceutical active compounds (PACs) has increased research interest because inadvertent exposure to these compounds in environmental water sources is associated with toxicity that can impact ecological and human health.[1] Therefore, selective detection and sensitive determination of PAC levels in environmental water testing is crucial.[2] Focused monitoring and evaluation of contaminants in the aquatic environment is generally regarded to be necessary for the protection of water quality and hence community health.[3] In recent years, advances in nanotechnology have emerged as an important industry for the manufacture of new nanomaterials.[4] Consequently, nanoparticles including metal oxide nanoparticles are widely found in a large variety of commercial and household products that are often dumped in landfills or sewage as wastes.[5] Titanium dioxide (TiO_2) nanoparticles have become a focal point of research due to their widespread daily use.[6] Upon irradiation with light, the exceptional band gap characteristic of this nanostructured semiconductor creates electron–hole pairs that result in the waste degradation cascade process.[7] These nanoparticles have attracted a substantial amount of attention in photocatalysis for the treatment of wastewater.[8] Cobalt tetroxide (Co_3O_4) nanoparticles play an important role in new energy battery technologies due to their excellent electrochemical stability, high energy density, and specific capacitance.[9] Their mass production and widespread use have gradually increased the risk of their environmental presence due to industrial and anthropogenic discharge.[10] Upon leaching release into ground and surface water, these nanoparticles with their characteristic high surface area-to-volume ratio exhibit a high adsorption capacity to bind numerous pharmaceutical compounds.[11] Furthermore, environmental effects such as pH and ionic strength changes could eventually desorb the compounds from the nanoparticle surface. Notably, the pH dictates the cationic, anionic, and zwitterionic speciation of pharmaceutical compounds as well as the surface charge of nanoparticles, thus affecting their interactions.[12] Generally, in a pH-controlled process, anionic compounds can be desorbed with an alkaline solution and cationic compounds can be desorbed with an acidic solution through electrostatic repulsion.[13,14] It has previously been reported by Dhiman and Sharma that pH plays a crucial role in ciprofloxacin adsorption onto ZnO nanoparticles.[15] It was determined that pH 8 is optimal for maximum adsorption based on the pK_a value of 6 for ciprofloxacin and the zero charge of 8.7 for ZnO. Moreover, Attia *et al.* observed the desorption of acidic pharmaceutical compounds (ibuprofen, naproxen,

Ottawa-Carleton Chemistry Institute, Department of Chemistry, Carleton University, Ottawa, ON K1S 5B6, Canada. E-mail: edward.lai@carleton.ca; Fax: +1 (613) 520 3749; Tel: +1 (613) 520 2600 ext. 3835

diclofenac-Na, and gemfibrozil having pK_a values around 4.1–4.9) from Fe_2O_3–zeolite composite surface at high pH levels, where the zeolite composite becomes negatively charged and electrostatic repulsion causes desorption of the pharmaceutical molecules.[16]

Furthermore, the ionic strength of the aqueous solution can enhance or suppress electrostatic interactions. An increase in the ionic strength will enhance adsorption by reducing the electrostatic repulsion between the adsorbent surface and the adsorbate molecules. On the other hand, if electrostatic interactions are attractive, increasing the ionic strength leads to desorption.[17] According to Gulley-Stahl *et al.*, this phenomenon can be explained by the increasing density of electrolyte ions at high ionic strengths, which decreases the diffuse layer thickness.[18] Furthermore, if electrolyte ions adsorb significantly, there would be an increase in competition for available surface sites, leading to desorption of pharmaceutical molecules. Bui *et al.* investigated the effect of varying ionic strength on the adsorption of four pharmaceutical compounds (carbamazepine, diclofenac, ibuprofen, and ketoprofen) onto porous silica. Based on the pK_a values of the compounds, at pH 5.3 carbamazepine is a neutral compound whereas diclofenac, ibuprofen, and ketoprofen are deprotonated and hence negatively charged. Consequently, carbamazepine adsorption slightly decreased as ionic strength increased from 0 to 50 mM.[19] As reported by Claussen *et al.*, dissolution of pharmaceutical compounds in water could be influenced by ionic strength; a higher ionic strength may cause neutral pharmaceuticals to be less soluble while ionizable acidic pharmaceuticals dissolve more readily.[20] Gao *et al.* observed that an increase in ionic strength enhanced the desorption of uncharged sulfamethazine to montmorillonite while the adsorption of anionic sulfamethazine increased.[21] Generally, one pharmaceutical compound does not exist alone in the environment but coexists with many other compounds. Competitive adsorption usually occurs between compounds with similar ionic charges for available active sites. Eventually, this competitive process could lead to the desorption of the previously adsorbed compounds.[22]

Response surface methodology (RSM) has been widely applied as an optimization method in scientific research.[23] It consists of several statistical techniques that can be used to model and analyze the effects of a variety of experimental parameters.[24] Using RSM, researchers can determine the best combination of parameters (*aka* factors) to produce optimum results.[25] By adopting this statistical approach, the number of experiment runs is reduced and the effects of each factor can be recognized.[26] Different studies have applied RSM to optimize electrochemical[27] and advanced oxidation[28] processes for drinking water treatment. Various process parameters including adsorbent dose, pH, metal ion concentration and reaction time have been successfully optimized for the biosorption of metals[29,30] and dyes.[31] Alidadi *et al.* investigated the effect of different parameters for optimizing the extraction of amoxicillin from an aqueous medium by using an emulsion liquid membrane based on the central composite design (CCD) model.[32] Another study successfully applied RSM using the Box–Behnken design (BBD) model to optimize fluoride adsorption onto apatite tricalcium phosphate.[33] To the best of our knowledge, statistical experimental design techniques have not been previously reported for the investigation of desorption processes. Specifically, the main objective of our present work was to apply RSM using the CCD model to investigate the desorption of a model PAC, mexiletine hydrochloride (MEX), from TiO_2 and Co_3O_4 nanoparticle surfaces. MEX is a well-established sodium channel blocker that acts on cardiac myocytes and neurons. It has long been used to treat some rare cardiopathy, epilepsy, neuromuscular diseases, and pain disorders in children.[34] This antiarrhythmic drug is also used to treat acute and chronic ventricular arrhythmias in adults.[35] Although mexiletine is extensively metabolized in humans *via* phase I and phase II reactions, approximately 10% of each mexiletine dose administered is recovered without modifications in urine.[36] The need of the current study also arises from inadvertent disposal of mexiletine due to shelf life expiry. While the US EPA – 40 CFR Part 439, Pharmaceutical Manufacturing Point, applies to process wastewater discharges resulting from the research and manufacture of pharmaceutical products,[37] environmental discharge through treatment plants cannot ensure minimizing the discharge of pharmaceutical waste completely.[38,39] Interesting findings had previously been reported on the binding of MEX with TiO_2, Co_3O_4 and ZnO nanoparticles.[40] MEX binding occurred through physical and chemical approaches between the pores of the external surface and within the pores of the internal surface of TMONPs. The Freundlich model showed the best fitting with a high value of R^2 and the minimum error values of SSE. It can be concluded that MEX·HCl bonded to heterogenous sites forming mono- and multilayers onto the surface of TMONPs as controlled by physisorption mechanism. The main mechanism was accomplished *via* electrostatic interaction and hydrogen bonding.

The combined effects of four independent variables, namely pH, metformin (MET) as competitive desorption agent, Na_2HPO_4 for ionic strength control, and $Na_2S_2O_5$ as reducing agent, on the desorption response were investigated in the present study. MET was selected as the competitive desorption agent in this study, on the basis of its pK_a of 12.4 (ref. 41) which is significantly higher than 9.5 for MEX.

2. Materials and methods

2.1. Preparation of samples and background electrolyte (BGE)

The stock solutions of MEX·HCl, MET·HCl, Na_2HPO_4, and $Na_2S_2O_5$ were prepared in deionized water. A calibration curve for MEX·HCl was constructed to determine the concentrations before and after adsorption–desorption experiments. A background electrolyte (BGE) solution was prepared by dissolving sodium phosphate dibasic in deionized water and adjusted with 1 M HCl or 1 M NaOH to the required pH level.

2.2. Batch adsorption–desorption experiments

Desorption studies were conducted to investigate the leaching behavior of mexiletine from TiO_2 and Co_3O_4 nanoparticles (adsorbents). Both TiO_2 (79.87 g mol^{-1}) nanopowder with particle size <50 nm and Co_3O_4 (240.80 g mol^{-1}) nanopowder with particle

Table 1 Coded and actual values of variables of the central composite design model

Variable	Actual values	Coded values	Real values at 5 coded levels				
			$-\alpha$	-1	0	1	$+\alpha$
pH	A	A	3	5	7	9	11
MET·HCl concentration	B (μg mL^{-1})	B	0	25	50	75	100
Na_2HPO_4 concentration	C (mM)	C	0	25	50	75	100
$Na_2S_2O_5$ concentration	D (mM)	D	0.0	0.1	0.43	0.75	1.00

size <50 nm were obtained from Millipore Sigma (Oakville, ON, Canada). Initially, an adsorption process was conducted in 20 mL of 0.02 mM (100 μg mL^{-1}) MEX·HCl containing 1 g L^{-1} (1 mg mL^{-1}) of the selected nanoparticles for MEX adsorption overnight. Upon completion of the adsorption process in 24 h, the contents were centrifuged at 300 rpm for 5 min. The supernatant was discarded, and the nanoparticles carrying the adsorbed MEX were air-dried overnight. A series of 30 desorption experiments with duplicate trials, as designed by CCD, were conducted with an appropriate amount of the dried nanoparticles carrying adsorbed MEX·HCl. In different bottles, the required volumes of desorbing solutions of MET·HCl (0–0.016 mM), Na_2HPO_4 (0–100 mM), and $Na_2S_2O_5$ (0.0–1.0 mM) were added at pH levels ranging from 3 to 11. After stirring for 24 hours to minimize particle–particle aggregation at the high ionic strength provided by Na_2HPO_4, the supernatant was analyzed using capillary electrophoresis (CE)[42] to determine the desorbed amount of MEX.

2.3. Determination of mexiletine hydrochloride by CE-UV

The adsorption/desorption samples were analyzed by capillary electrophoresis (G1600AX CE system, Agilent Technologies, Santa Clara, USA) equipped with a fused silica capillary of 28 cm length from the inlet to the detection window. To display the migration time of analytes, a diode array detector (DAD) was set up at three wavelengths of 200, 230 and 254 nm to monitor the UV spectral characteristics of different PACs. The capillary was filled with 75 mM Na_2HPO_4 BGE adjusted to pH 9.4. The samples were injected hydrodynamically at 20 mbar for 10 s. With an applied voltage of 10 kV, the capillary was equilibrated at a temperature of 20 °C. A calibration curve was constructed for determining the unknown concentrations of MEX after desorption from TiO_2 and/or Co_3O_4. The % desorption was calculated according to:

$$\%\ \text{desorption} = \frac{[\text{MEX}]_{\text{des}}}{[\text{MEX}]_{\text{ads}}} \times 100 \quad (1)$$

where $[\text{MEX}]_{\text{des}}$ and $[\text{MEX}]_{\text{ads}}$ represent the desorbed and adsorbed amounts of MEX, respectively. Triplicate adsorption/desorption runs were carried out to determine the reproducibility of the CE-DAD analysis results and their standard deviation (SD) was calculated to verify the analytical precision.

2.4. Experimental design and statistical analysis

Design Expert 22.0.1 statistical software (Stat-Ease, Minneapolis, MN, USA) was used for the initial design of experiments (DOE) and subsequent data analysis. Response surface methodology (RSM) was used with central composite design (CCD) to optimize the variables affecting the % desorption of MEX from the surfaces of both TiO_2 and Co_3O_4 nanoparticles. In order to determine the optimum desorption conditions, four independent variables were considered: pH level, MET as competing desorption agent, Na_2HPO_4 for ionic strength control, and $Na_2S_2O_5$ as reducing agent. Optimization experiments were performed on the four factors, each factor taking five different values as shown in Table 1. The CCD consisted of 2^n factorial runs, $2n$ axial runs, as well as n_C center runs. The total number of experimental runs (N) conducted was therefore:

$$N = 2^n + 2n + n_C \quad (2)$$

where n is number of independent variables (factors). The total number of runs in this study based on the four independent variables ($n = 4$) was:

$$N = 2^4 + 2(4) + 6 = 30 \text{ runs} \quad (3)$$

A total of 30 experiments were conducted in random order to avoid biases. The axial point ensures rotatability, whereas the center point ensures reproducibility and defines experimental errors. Table 1 presents the real values of the four variables at 5 coded levels in the CCD model.

3. Results and discussion

3.1. Central composite design (CCD) model

In analytical separation, challenges may arise from insufficient resolution between adjacent CE peaks for accurate height measurement.[43] To address these challenges, the response surface methodology (RSM) can be used to optimize all three experimental parameters. Using this statistical method, the relationships between several explanatory variables and one or more response variables can be explored in the least amount of time. It is possible to screen many parameters simultaneously to determine which ones are significant factors in the separation process.[44] A statistical approach of CCD was employed to optimize MEX desorption from both TiO_2 and Co_3O_4 nanoparticles using a combination of thirty experimental runs. The CCD model required 16 factorial runs, 8 axial runs and 6 center runs for optimizing the desorption process. This large number of experiments, encompassing a wide range of conditions, was

essential to determining the optimal factors for MEX desorption. Eqn (4) and (5) were used to calculate the % desorptions of MEX, shown as responses in Table 2. The experimental data was also analyzed by CCD to determine if the linear or quadratic model would be better for predicting the maximum desorption percentage. The quadratic model (second-degree polynomial function) showed a high R^2 value and a p-value of less than 0.05. The model also showed a low standard deviation and a high F- and regression coefficient values. Thus, the quadratic model was chosen for the calculation of the predicted values of % desorption and its relationship to the independent variables. The validity of the proposed model, as well as the agreement between the experimental and predicted values of % desorption, could then be evaluated using an analysis of variance (ANOVA) next.

Calculating the predicted values of % desorption required the determination of the regression coefficients (as predictors) of a quadratic model. By altering the desorption process factors, the CCD analysis normalized the experimental data through multiple regression analysis. A polynomial second order (quadratic) model was then produced by calculating the regression coefficients and subtracting any/all non-significant effects. Using the general quadratic model equation and the regression coefficients determined, two coded models eqn (4) and (5) were generated for MEX desorption from TiO_2 and Co_3O_4 nanoparticles:

$$\begin{aligned}\%\ \text{desorption}\ (TiO_2) = {} & -16.98 + 2.73A + 1.01B + 0.50C \\ & + 40.22D - 0.03AB - 0.02AC + 0.33AD \\ & + 0.002BC - 0.05BD + 0.04CD \\ & - 0.35A^2 - 0.007B^2 \\ & - 0.003C^2 - 47.71D^2 \end{aligned} \quad (4)$$

$$\begin{aligned}\%\ \text{desorption}\ (Co_3O_4) = {} & 33.67 - 8.07A + 0.62B + 0.68C \\ & + 13.97D - 0.04AB - 0.03AC + 1.63AD \\ & + 0.001BC - 0.12BD + 0.16CD \\ & - 0.23A^2 - 0.007B^2 \\ & - 0.003C^2 - 21.20D^2 \end{aligned} \quad (5)$$

By replacing the coded variables with the actual variables studied (pH, MET·HCl concentration, Na_2HPO_4 concentration, and $Na_2S_2O_5$ concentration), the following equations were

Table 2 Central composite design matrix of process factors for MEX·HCl desorption

			Independent design factors				Responses					
							Desorption from TiO_2			Desorption from Co_3O_4		
Std run	Rand. run	CCD position	pH	Competitive [MET·HCl] μg mL^{-1}	Ionic strength [Na_2HPO_4] mM	Reducing agent [$Na_2S_2O_5$] mM	Des. (%) exp	S. D.	Des. (%) pre	Des. (%) exp	S. D.	Des. (%) pre
1	14	Factorial	5	25	25	0.1	17.35	0.86	18.92	29.41	0.16	30.52
2	30	Factorial	9	25	25	0.1	5.96	0.35	6.05	15.36	0.16	13.86
3	20	Factorial	5	75	25	0.1	31.44	0.43	31.46	36.78	0.56	38.39
4	1	Factorial	9	75	25	0.1	12.79	0.86	12.63	30.42	0.32	30.65
5	17	Factorial	5	25	75	0.1	28.12	0.49	26.93	43.13	0.59	44.62
6	28	Factorial	9	25	75	0.1	11.14	0.32	11.08	23.39	0.43	22.86
7	16	Factorial	5	75	75	0.1	42.62	0.65	44.14	57.53	0.32	56.31
8	26	Factorial	9	75	75	0.1	21.49	0.43	22.34	42.47	0.32	43.47
9	23	Factorial	5	25	25	0.75	20.25	0.32	19.56	32.09	0.99	32.56
10	27	Factorial	9	25	25	0.75	8.65	0.16	7.53	19.71	0.28	20.15
11	7	Factorial	5	75	25	0.75	29.78	0.71	30.39	34.43	0.32	34.05
12	15	Factorial	9	75	25	0.75	10.31	0.32	12.42	30.08	0.43	30.56
13	25	Factorial	5	25	75	0.75	28.16	1.06	28.84	52.51	0.59	51.76
14	12	Factorial	9	25	75	0.75	13.21	0.28	13.83	34.43	0.32	34.25
15	8	Factorial	5	75	75	0.75	44.28	0.97	44.35	54.51	0.32	57.07
16	29	Factorial	9	75	75	0.75	23.15	0.49	23.40	50.50	0.43	48.48
17	13	Axial	3	50	50	0.425	46.41	0.71	45.95	63.22	0.59	60.96
18	3	Axial	11	50	50	0.425	12.38	0.32	12.12	34.43	0.71	35.71
19	19	Axial	7	0	50	0.425	5.75	0.28	7.19	15.02	0.99	15.98
20	9	Axial	7	100	50	0.425	31.44	0.99	29.29	39.12	0.65	38.08
21	24	Axial	7	50	0	0.425	17.35	0.71	17.25	21.38	0.81	20.37
22	4	Axial	7	50	100	0.425	36.41	0.71	36.24	51.84	0.56	52.39
23	2	Axial	7	50	50	0	26.47	0.86	25.42	39.45	0.71	38.47
24	22	Axial	7	50	50	1	20.20	0.71	19.57	40.46	0.86	40.71
25	11	Center	7	50	50	0.425	35.17	0.81	34.59	45.81	1.01	44.60
26	21	Center	7	50	50	0.425	35.58	1.23	34.59	44.14	0.86	44.60
27	5	Center	7	50	50	0.425	34.34	1.49	34.59	45.48	1.17	44.60
28	10	Center	7	50	50	0.425	33.92	1.39	34.59	42.13	1.33	44.60
29	6	Center	7	50	50	0.425	33.09	1.41	34.59	44.81	1.01	44.60
30	18	Center	7	50	50	0.425	34.34	1.49	34.59	45.14	1.44	44.60

obtained for calculating the predicted values of the % desorption of MEX from TiO_2 and Co_3O_4 nanoparticles:

$$\%\ \text{desorption from } TiO_2 = -16.98 + 2.73 \times \text{pH} + 1.01 \times [\text{MET}\cdot\text{HCl}] + 0.50 \times [Na_2HPO_4] + 40.22 \times [Na_2S_2O_5] - 0.03 \times \text{pH} \times [\text{MET}\cdot\text{HCl}] - 0.02 \times \text{pH} \times [Na_2HPO_4] + 0.33 \times \text{pH} \times [Na_2S_2O_5] + 0.002 \times [\text{MET}\cdot\text{HCl}] \times [Na_2HPO_4] - 0.05 \times [\text{MET}\cdot\text{HCl}] \times [Na_2S_2O_5] + 0.04 \times [Na_2HPO_4] \times [Na_2S_2O_5] - 0.35 \times \text{pH}^2 - 0.007 \times [\text{MET}\cdot\text{HCl}]^2 - 0.003 \times [Na_2HPO_4]^2 - 47.71 \times [Na_2S_2O_5]^2 \quad (6)$$

$$\%\ \text{desorption from } Co_3O_4 = 33.67 - 8.07 \times \text{pH} + 0.62 \times [\text{MET}\cdot\text{HCl}] + 0.68 \times [Na_2HPO_4] + 13.97 \times [Na_2S_2O_5] + 0.04 \times \text{pH} \times [\text{MET}\cdot\text{HCl}] - 0.03 \times \text{pH} \times [Na_2HPO_4] + 1.63 \times \text{pH} \times [Na_2S_2O_5] + 0.001 \times [\text{MET}\cdot\text{HCl}] \times [Na_2HPO_4] - 0.12 \times [\text{MET}\cdot\text{HCl}] \times [Na_2S_2O_5] + 0.16 \times [Na_2HPO_4] \times [Na_2S_2O_5] + 0.23 \times \text{pH}^2 - 0.007 \times [\text{MET}\cdot\text{HCl}]^2 - 0.003 \times [Na_2HPO_4]^2 - 21.20 \times [Na_2S_2O_5]^2 \quad (7)$$

These two mathematical quadratic models, eqn (6) and (7) where each concentration is represented by a pair of square brackets, unambiguously identify the individual and interaction impacts of the variables studied. The predicted values calculated from the two models ranged from 6.05% to 45.95% for TiO_2 and 13.86% to 60.96% for Co_3O_4. In comparison, the results in Table 2 indicated that the effect of the four factors on the values of the experimental % desorption of MEX ranged from 5.95% ± 0.35% to 46.41% ± 0.71% for TiO_2 nanoparticles, and 15.36% ± 0.16% to 63.22% ± 0.59% for Co_3O_4 nanoparticles. As expected, the predicted range of values are consistent with the experimental range of results for each TMONP. Overall, the ranges obtained for TiO_2 nanoparticles are lower in values than those obtained for Co_3O_4 nanoparticles. This clear distinction between the two TMONPs can be explained by their different physicochemical properties. For the sake of chemical analysis, it would be more difficult to recover MEX by desorption from TiO_2 than Co_3O_4 nanoparticles, using the four factors studied.

3.2. ANOVA and determination of significant effects

Analysis of variance (ANOVA), contour plots, and response surfaces were used to evaluate the validity of the selected model as well as the agreement between experimental and predicted values. In addition, the effects of factor interactions on the % desorption responses were examined. ANOVA is a hypothesis testing technique based on the *F*-test, *p*-values, and lack-of-fit statistical calculations to study the validity of a selected model. Statistical significance is determined by the *p*-values of the collected results, which should be <0.05 with a 95% confidence level.

3.2.1. Validity of the quadratic model for predicting the % desorption. The validity of a selected model will be determined based on the *F*-value, *p*-value, the lack of fit test, the actual total sum of squares (TSS) value, and correlation coefficient (R^2) value. The correlation coefficients (R^2) are used to assess the quality of fitted models, and the *F*-value confirms the expansion of regression coefficients at the 5% confidence level. As shown in Tables 3 and 4, the quadratic regression model has high *F*-values of 144.1 and 115.0 for TiO_2 and Co_3O_4, respectively, with *p*-values <0.05 indicating that there is only a 0.01% chance that this large *F*-value could occur due to noise. In addition, the actual TSS values of 3908.45 and 4218.07 for TiO_2 and Co_3O_4 respectively are very close to the sum of squares (SS) values of the model, indicating that the quadratic model is significant. Also, the model has very high adjusted R^2 values of 0.986 and 0.982 and predicted R^2 values of 0.960 and 0.950 for TiO_2 and Co_3O_4 nanoparticles, respectively. The predicted R^2 values are in reasonable agreement with the adjusted R^2 values, and hence the difference is less than 0.2 as mentioned in the software explaining ANOVA. Moreover, the adequate precision ratios for TiO_2 and Co_3O_4 were 40.55 and 41.15, respectively; precision ratios greater than 4 indicate adequate model discrimination. For most factors, the *p*-values are less than 0.050. Furthermore, the lack of fit test is not significant, resulting in a *p*-value greater than 0.05 and *F*-values of 3.34 and 2.82 for TiO_2 and Co_3O_4 respectively. As a result of the large *F*-values, there is a 9.76% and 13.16% chance for TiO_2 and Co_3O_4 respectively that the lack of fit value could be the result of noise. Accordingly, a quadratic response surface model was selected to fit the experimental results of the % desorption from TiO_2 and Co_3O_4.

As evaluated by the *p* values, the significance of RSM-CCD results was <0.05 with a 95% confidence level representing a significant correlation between the experimental and predicted values. Nevertheless, the effects of the four individual factors were different for the two adsorbents. TiO_2 exhibited the order of pH > MET concentration > Na_2HPO_4 concentration > $Na_2S_2O_5$ concentration, as indicated by the *F*-values of 886, 378, 279, and 1.86, respectively. On the other hand, Co_3O_4 exhibited the order Na_2HPO_4 concentration > pH > MET concentration > $Na_2S_2O_5$ concentration, as indicated by the *F*-values of 587, 365, 280, and 24. The results indicated that the % desorption of MEX from TiO_2 and Co_3O_4 could be increased by decreasing the pH level from 11 to 3 in water sample pretreatment. Also, as the concentration Na_2HPO_4 and hence ionic strength increase, electrostatic interactions decrease, resulting in more MEX desorption. Furthermore, MET competition with active sites on TiO_2 and Co_3O_4 surfaces enhances MEX desorption. However, the change in $Na_2S_2O_5$ concentration had very minimal effect on the % desorption. In conclusion, based on the 46% desorption of mexiletine from TiO_2 being less than the 63% desorption from Co_3O_4, the binding interactions between MEX and TiO_2 are stronger than MEX interactions with Co_3O_4.

Table 3 ANOVA for response 1: desorption from TiO_2 nanoparticles

Source	Sum of squares (SS)	Mean square	DF[a]	*F*-Value	*p*-Value
Model (quadratic) (predicted value)	3908.45	279.17	14	144.11	<0.0001
Corrected total sum of squares (TSS) (actual value)	3937.51	135.77	29		
Lack of fit	25.28	2.53	10	3.34	0.0976
A-pH	1716.70	1716.70	1	886.19	<0.0001
B-Competing agent (metformin)	732.61	732.61	1	378.19	<0.0001
C-Ionic strength (Na_2HPO_4)	540.55	540.55	1	279.04	<0.0001
D-Reducing agent ($Na_2S_2O_5$)	3.61	3.61	1	1.86	0.1926
AB	35.40	35.40	1	18.28	0.0007
AC	8.85	8.85	1	4.57	0.0494
BC	21.86	21.86	1	11.28	0.0043
AD	0.7225	0.7225	1	0.3730	0.5505
BD	2.89	2.89	1	1.49	0.2408
CD	1.63	1.63	1	0.8392	0.3741
A^2	53.91	53.91	1	27.83	<0.0001
B^2	466.95	466.95	1	241.05	<0.0001
C^2	107.65	107.65	1	55.57	<0.0001
D^2	349.56	349.56	1	180.45	<0.0001
Residual	29.06	1.94	15		
Pure error	3.78	0.7562	5		

Predicted $R^2 = 0.960$
Adjusted $R^2 = 0.986$
Adequate precision = 40.55

[a] Degree of freedom (DF) is the number of estimated parameters used to compute the source's sum of squares. The DF for the terms was 1 as the sum of squares equals the mean square (divided by DF = 1). The DF for the model equals 14 as obtained by dividing the sum of squares (3908.4) by the mean square (279.17).

Table 4 ANOVA for response 2: desorption from Co_3O_4 nanoparticles

Source	Sum of squares (SS)	Mean square	DF	*F*-Value	*p*-Value
Model (quadratic) (predicted value)	4218.07	301.29	14	115.00	<0.0001
Corrected total sum of squares (TSS) (actual value)	4257.37	146.80	29		
Lack of fit	33.39	3.34	10	2.82	0.1316
A-pH	956.34	956.34	1	365.02	<0.0001
B-Competitive (metformin)	732.61	732.61	1	279.62	<0.0001
C-Ionic strength (Na_2HPO_4)	1537.60	1537.60	1	586.87	<0.0001
D-Redox ($Na_2S_2O_5$)	62.86	62.86	1	23.99	0.0002
AB	79.66	79.66	1	30.40	<0.0001
AC	26.01	26.01	1	9.93	0.0066
AD	18.06	18.06	1	6.89	0.0191
BC	14.63	14.63	1	5.58	0.0321
BD	40.64	40.64	1	15.51	0.0013
CD	26.01	26.01	1	9.93	0.0066
A^2	24.27	24.27	1	9.26	0.0082
B^2	539.35	539.35	1	205.86	<0.0001
C^2	118.09	118.09	1	45.07	<0.0001
D^2	69.06	69.06	1	26.36	0.0001
Residual	39.30	2.62	15		
Pure error	5.91	1.18	5		

Predicted $R^2 = 0.982$
Adjusted $R^2 = 0.950$
Adequate precision = 41.15

3.2.2. The agreement between experimental and predicted values of % desorption. The actual data and predicted values of % desorption of MEX from TiO_2 and Co_3O_4 nanoparticles have been presented in Table 2 above. A comparison between the predicted and actual results is shown in Fig. 1(a and b). There is a significant correlation between observed and expected values as indicated by the dispersion of correlation data points along a straight line.

An analysis of normal probability plots was performed to evaluate the normality of the data. Fig. 2(a and b) show the normal probability plot of residuals for % desorption from TiO_2 and Co_3O_4 nanoparticles. Both % desorption plots are linear, which indicates that errors are normally distributed.

3.3. Desirability function for optimization

The % desorption goal for TiO_2 and Co_3O_4 nanoparticles was set to attain the optimum point. After validating the model, desirability function was used to determine the conditions that could lead to the optimum response values by optimizing the independent variables. The desirable range is between 0 and 1; zero represents an unacceptable configuration, while 1 represents the ideal configuration for the selected response.[45] It was found that at pH 3, 50 mM Na_2HPO_4, 50 μg mL^{-1} MET·HCl and 0.425 M $Na_2S_20_5$, desirability was 0.999 for both % desorptions from TiO_2 and Co_3O_4 hence confirming the optimum value for each factor. As illustrated by the 3D and counter plots shown in Fig. 5 and 6, the % desorptions from TiO_2 and Co_3O_4 were optimized to maximum values at 46.41% ± 0.71 and 63.22% ± 0.59 respectively under these conditions. Fig. 3(a and b) illustrates the electropherogram obtained from CE, for maximum % desorptions from TiO_2 and Co_3O_4 respectively. These two pharmaceutical compounds were separated in the migration order of metformin (2.65 min) and mexiletine (2.90 min), with good resolution between the two peaks down to the baseline.

Note that the % desorption could not be easily determined by CE-DAD analysis at the PAC concentration levels tested in the present study if microparticles or milliparticles were chosen. Only nanoparticles offered a sufficiently high specific surface area (cm^2 mg^{-1}) to result in a measurable change in the high working concentration of MEX required by the relatively low sensitivity of CE-DAD analysis, to yield experimental data of adequate signal-to-noise ratio values for reliable statistical significance evaluation.

3.4. Effect of factors on the responses

The quadratic models represented in eqn (6) and (7) show the effects of four factors (pH, MET·HCl concentration, Na_2HPO_4 concentration, and $Na_2S_2O_5$ concentration) on the % desorption of MEX from TiO_2 and Co_3O_4 nanoparticles, respectively. The ANOVA calculation results for % desorption from TiO_2 nanoparticles in Table 3 show significant effects of pH, MET·HCl concentration, Na_2HPO_4 concentration, pH : [MET·HCl], and [MET·HCl] : [Na_2HPO_4]. The individual factors descend in the order of pH > MET concentration > Na_2HPO_4 concentration > $Na_2S_2O_5$ concentration, as indicated by the *F*-values of 886, 378, 279, and 1.86. For % desorption of MEX from Co_3O_4 nanoparticles in Table 4, all the individual factors and their interactions have a significant effect as indicated by *p*-values <0.05. However, the individual factors descend in a different order as Na_2HPO_4 concentration > pH > MET concentration > $Na_2S_2O_5$ concentration as indicated by the *F*-values of 587, 365, 280, and 24. It was noted that $Na_2S_2O_5$

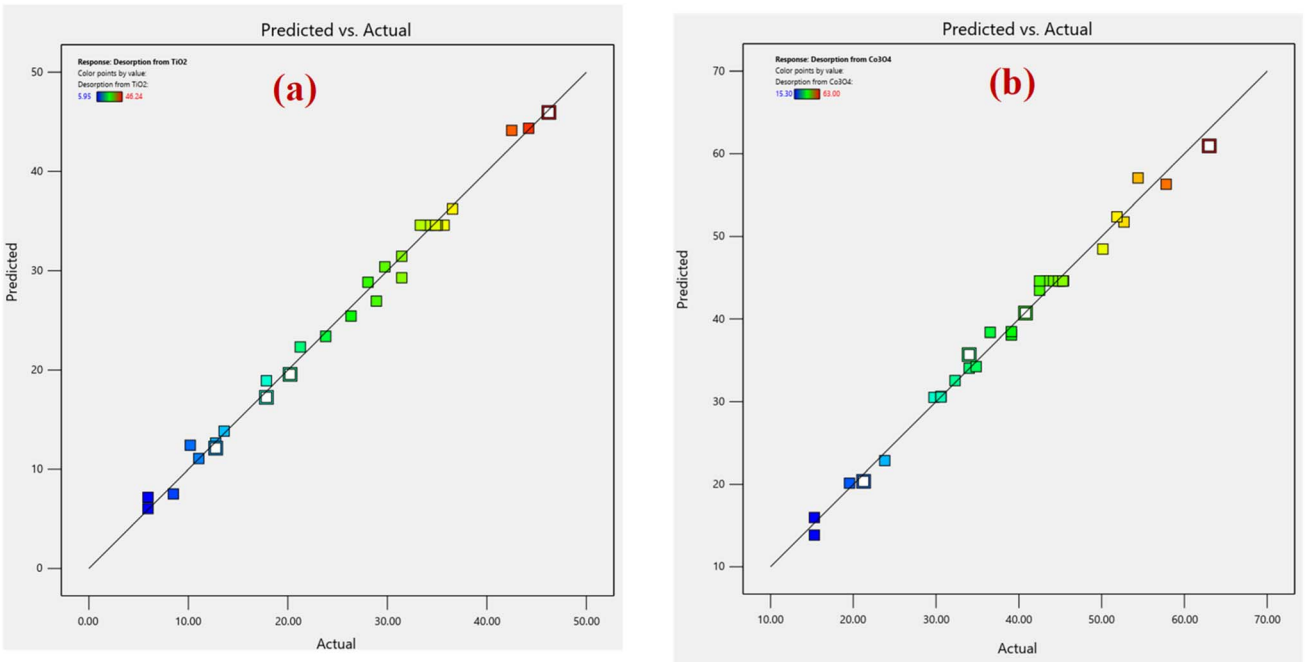

Fig. 1 Comparison of predicted *versus* actual data of RSM-CCD for (a) % desorption from TiO_2 nanoparticles, and (b) % desorption from Co_3O_4 nanoparticles.

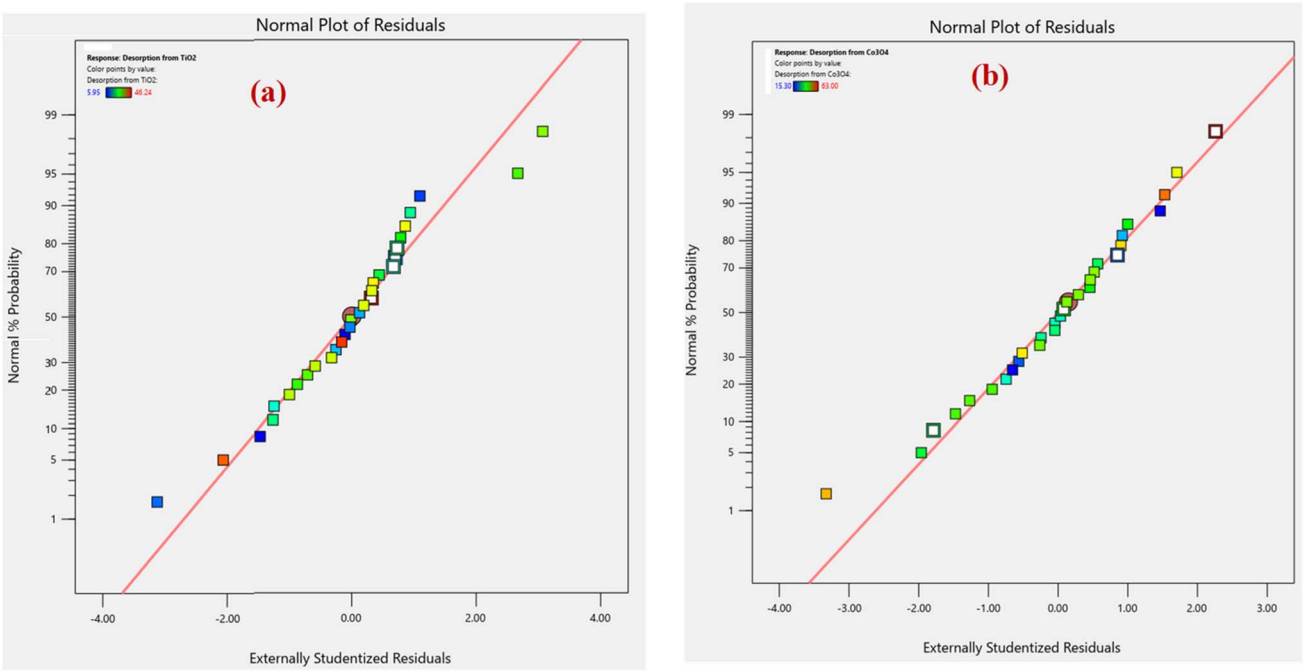

Fig. 2 Normal CCD plot of residuals data: (a) % desorption from TiO_2 nanoparticles, and (b) % desorption from Co_3O_4 nanoparticles.

concentration has the lowest effect on the % desorption for both types of nanoparticles, as indicated by the low *F*-values of 1.86 and 24. This suggests that redox interactions between $Na_2S_2O_5$ and TiO_2 or Co_3O_4 nanoparticles did not play any important role in the MEX desorption.

3.4.1. Effect of pH. The desorption–adsorption process of pharmaceutical compounds (bases, acids, and zwitterions) is highly dependent on the properties of each adsorbent, the chemical structure of every compound, and the pH of solution.[46] Based on the point of zero charge (PZC) of the nanoparticles, pK_a of the compound, and pH of the medium, the acidic/basic functional groups in the PAC molecule will behave differently. It was previously reported that the pH level; affected the degree of deprotonation/protonation, and hence the ratio of the neutral

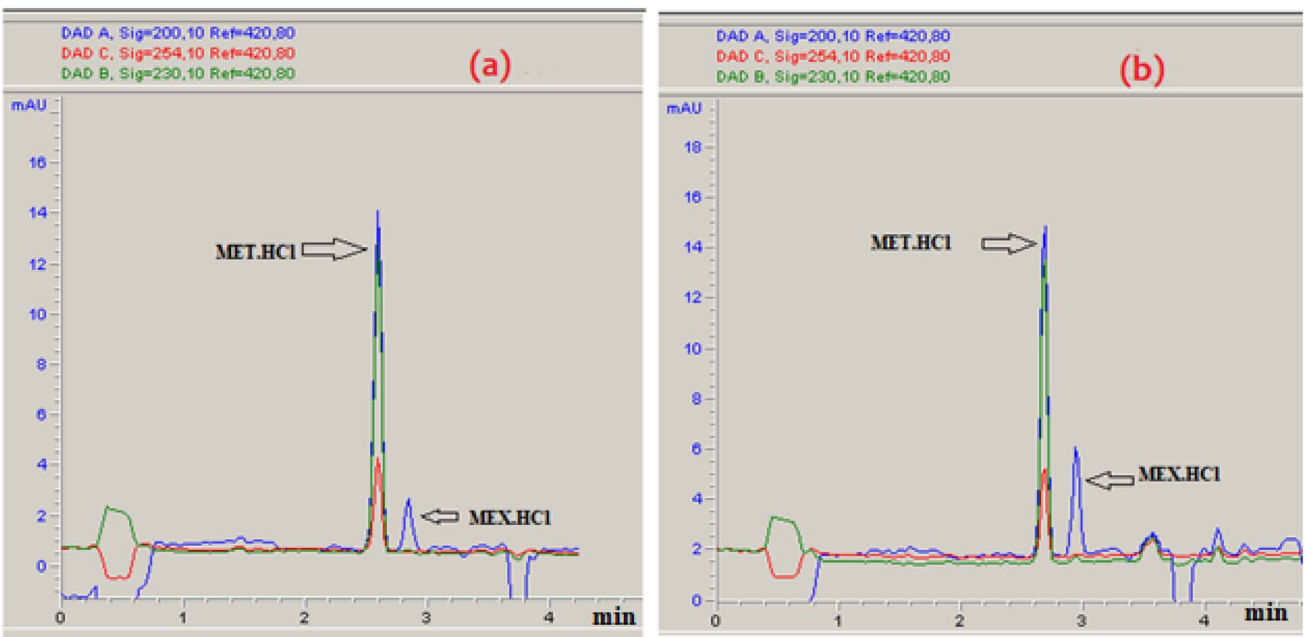

Fig. 3 Electropherogram of maximum % desorption of MEX from (a) TiO_2, and (b) Co_3O_4 nanoparticles. The first peak represents metformin hydrochloride and second peak mexiletine hydrochloride based on their characteristic migration times.

molecule to all ionized forms.[47] As pH dictated the zeta potential of each TMONP, it had a direct influence on the adsorption of PACs. Three-dimensional (3D) and contour plots of the model can be used to visualize the relationship between % desorption and all studied factors.[48] In 3D and contour plots, red indicates the highest response value while blue indicates the lowest response value. Fig. 5 and 6(a–c) demonstrate an elliptical distribution of contours, indicating a significant interaction between pH, ionic strength, and competitive desorption agent (MET) for MEX desorption from TiO_2 and Co_3O_4 nanoparticles. Apparently, the % desorption increased, going from pH 11 to pH 3. This could be explained by the pK_a of MEX being 9.5 and the PZCs of TiO_2 and Co_3O_4 being 6.7 and 7.3. As reported previously, at pH 3, the basic amino group ($-NH_2$) of MEX can accept protons[49] leading to the predominance of its conjugate acid ($MEX{\cdot}H^+$). Also, the surface of both TiO_2 and Co_3O_4 carries a positive charge at pH 3 ($pH < pH_{pzc}$). Hence, the surfaces of TiO_2 and Co_3O_4 nanoparticles and MEX are positively charged resulting in a repulsive interaction and causing the desorption of MEX from the the adsorbent surfaces. Increasing the pH value in the medium up to pH 11 enhanced the presence of the anion form of MEX and the TiO_2 and Co_3O_4 nanoparticle surfaces will become more negative ($pH > pH_{pzc}$) which would also increase the % desorption. However, the % desorption from TiO_2 and Co_3O_4 was observed to decrease to 12.38% ± 0.32% and 43.43% ± 0.71% respectively because pH 11 was only 1.5 units higher than the pK_a of 9.5 for MEX. The electropherograms obtained at pH 11 for desorption from TiO_2 and Co_3O_4 are represented in Fig. 4(a and b) respectively even though those obtained at pH 3 are not shown here. This could be attributed to the adsorption of MEX onto the adsorbent surfaces due to coordination bonding. Overall, the desorption rate will vary depending on the type and strength of interactions between the PAC molecule and the adsorbent surface.

3.4.2. Effect of ionic strength. The effects of ionic strength on % desorption from TiO_2 is shown in Fig. 5(a, d and e), and from Co_3O_4 in Fig. 6(a, d and e). Changes in the ionic strength factor showed a significant effect with a *p*-value <0.001. By increasing the concentration of Na_2HPO_4 the electrostatic interactions between $MEX{\cdot}HCl$ and TiO_2 or Co_3O_4 decreased and the negatively charged phosphate ions could compete for the active sites onto the surface of each adsorbent. Phosphate speciation in different water conditions may have an impact on the desorption process. As reported by Bian *et al.* the dominant phosphate species in solution varies with pH.[50] At pH 3 the dominant phosphate species is $H_2PO_4^-$ and by increasing the pH, phosphate ions deprotonate to form the dominant species of PO_4^{3-} at pH 14. This enhances the % desorption from the adsorbent surface due to a decrease in the electrostatic interaction as the concentration of $MEX{\cdot}H^+$ cations decreases.

3.4.3. Effect of metformin as competing agent. As discussed previously, MET showed a significant binding affinity to both TiO_2 and Co_3O_4 nanoparticles. Fig. 5(b) and 6(b) showed the effects of MET as a competing agent. The presence of MET led to an increase in the % desorption of MEX from TiO_2 and Co_3O_4 nanoparticles. MET could compete for the active sites on TiO_2 and Co_3O_4 surfaces, causing the desorption of MEX. The mechanism behind the competitive desorption of MEX by MET can theoretically be explained by the pK_a of 12.4 for MET which is significantly higher than 9.5 for MEX. At any environmental pH level, MET molecules are more positively charged than MEX molecules. Electrostatic attraction thus renders a strong

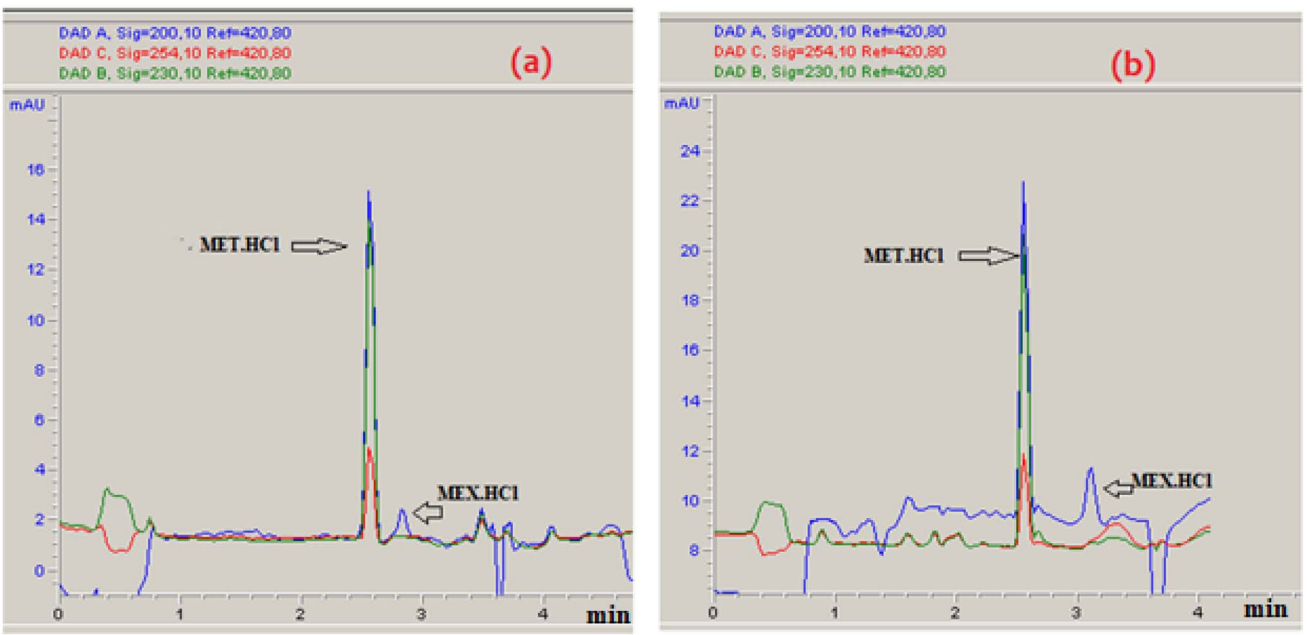

Fig. 4 Electropherogram of $MEX{\cdot}HCl$ desorbed from (a) TiO_2, and (b) Co_3O_4 nanoparticles at pH 11 using 50 mM Na_2HPO_4, 50 μg mL^{-1} $MET{\cdot}HCl$, and 0.425 mM $Na_2S_2O_5$. The first peak represents metformin hydrochloride and second peak mexiletine hydrochloride based on their characteristic migration times.

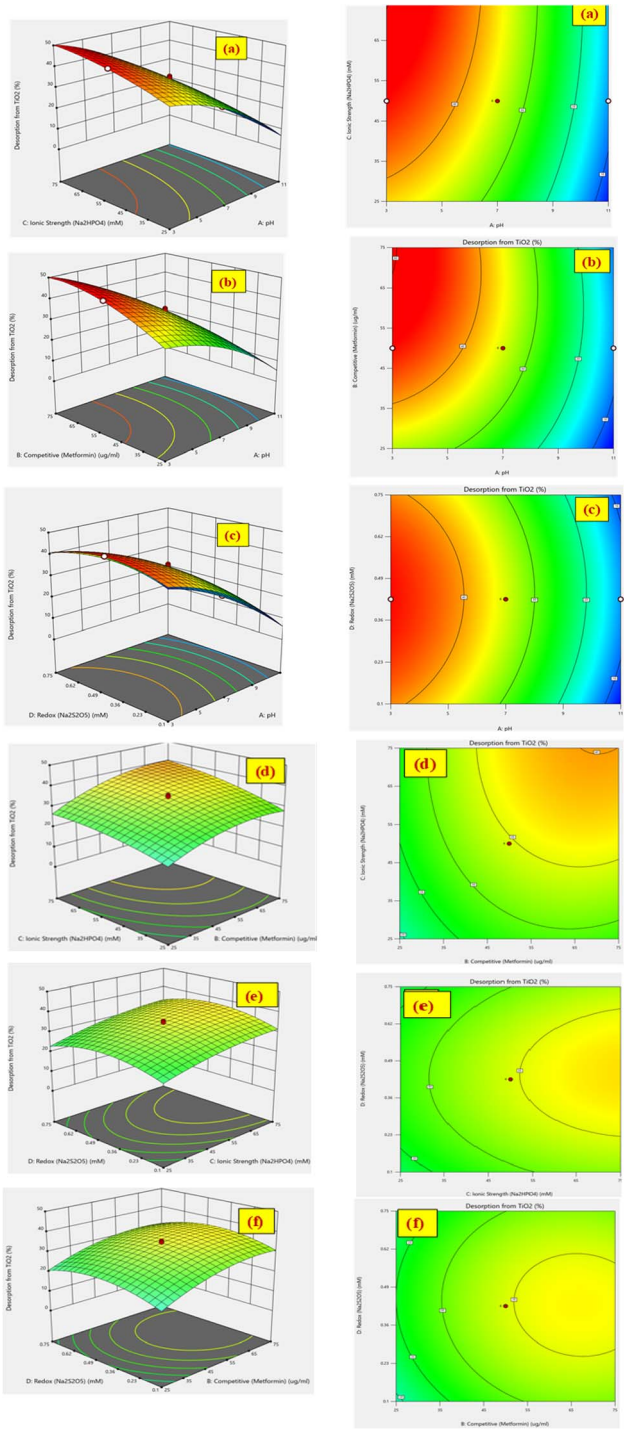

Fig. 5 RSM plot (3-D) and corresponding contour plot (2-D) showing the combined effect of main factors: (a) pH and [Na_2HPO_4] (mM), (b) pH and [MET·HCl] (μg mL^{-1}), (c) pH and [$Na_2S_2O_5$], (mM), (d) [Na_2HPO_4] (mM) and [MET·HCl] (μg mL^{-1}), (e) [$Na_2S_2O_5$] (mM) and [MET·HCl] (μg mL^{-1}), and (f) [$Na_2S_2O_5$] (mM) and [Na_2HPO_4] (mM) on the % desorption of MEX·HCl from TiO_2 nanoparticles.

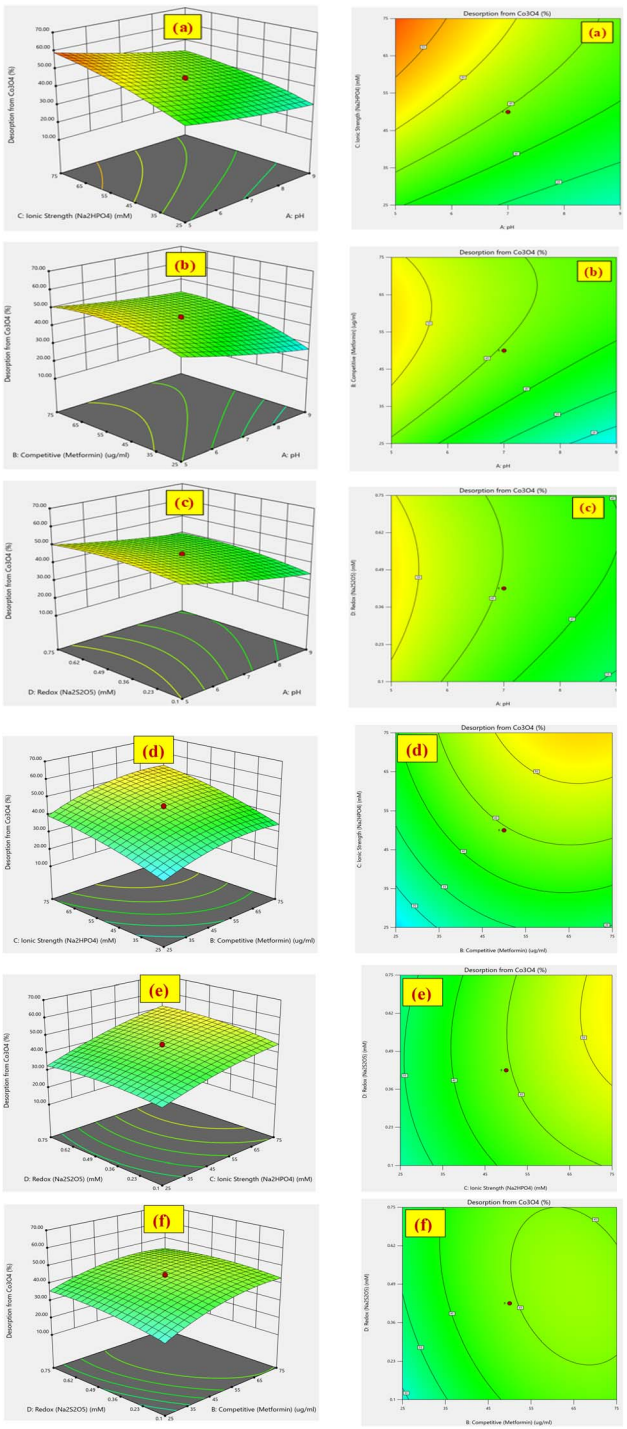

Fig. 6 RSM plot (3-D) and corresponding contour plot (2-D) showing the combined effect of main factors: (a) pH and [Na_2HPO_4] (mM), (b) pH and [MET·HCl] (μg mL^{-1}), (c) pH and [$Na_2S_2O_5$] (mM), (d) [Na_2HPO_4] (mM) and [MET·HCl] (μg mL^{-1}), (e) [Na_2HPO_4] (mM) and [$Na_2S_2O_5$] (mM), and (f) [$Na_2S_2O_5$] (mM) and [MET·HCl] (μg mL^{-1}) on the % desorption of MEX·HCl from Co_3O_4 nanoparticles.

binding potential due to the negative charge on TiO_2 nanoparticle surfaces attracting the positive MET molecules. This attraction is less pronounced with Co_3O_4 nanoparticles owing to its variable charge states. Weak electrostatic interactions of MEX with TiO_2 and Co_3O_4 established a lesser tendency for binding with both nanoparticles due to a lack of strong ionic character. As evidenced from our empirical adsorption experiments, MET exhibited strong interactions with both TiO_2 and Co_3O_4 nanoparticles, which was useful in the desorption-based release of MEX from these two TMONPs.

3.4.4. Effect of $Na_2S_2O_5$. The plots in Fig. 5(c) and 6(c) showed the effect of $Na_2S_2O_5$ as a reducing agent. Changes in the concentration of $Na_2S_2O_5$ have a minimal effect on the % desorption of MEX from TiO_2 nanoparticles, as indicated by the high *p*-value 0.1926. Furthermore, the *p*-values for the interaction effects (pH and [MET·HCl], pH and [$Na_2S_2O_5$], [MET·HCl] and [$Na_2S_2O_5$], [Na_2HPO_4] and [$Na_2S_2O_5$]) were all higher than 0.050 indicating that the effects of this reducing agent on the % desorption of MEX from the nanoparticles were minimal.

4. Conclusion

In this study, RSM using the CCD model was applied to maximize the desorption percentages of MEX from TiO_2 and Co_3O_4 nanoparticles. All data analysis and design of experiments were performed using Design Expert statistical software. To determine the optimal desorption conditions, four independent factors were studied: pH, concentration of MET as competitive desorption agent, concentration of Na_2HPO_4 for ionic strength control, and concentration of $Na_2S_2O_5$ reducing agent. The ANOVA results indicated that the quadratic model was good for estimating the predicted values of % desorption and analyzing the relationship between the independent factors. There was a positive correlation between these four factors and the experimental desorption results obtained for MEX·HCl, ranging from 5.9% to 46.2% for TiO_2 nanoparticles and 15.3% to 63.0% for Co_3O_4 nanoparticles. Using the mathematical quadratic model, the predicted desorption values for TiO_2 and Co_3O_4 ranged from 6.0% to 45.9% for TiO_2 and 13.3% to 63.0% for Co_3O_4. Overall, it would be more difficult to quantitatively recover MEX by desorption from TiO_2 than Co_3O_4 nanoparticles, using the four factors studied. For the most accurate determination of PAC levels in environmental water testing, it would be crucial to consider the existence of various TMONPs and their potential binding with PACs. Further research will be needed to optimize more chemical desorption parameters, in the presence of all major TMONPs as found in environmental water sources. The scope of our future study will explore the dynamic relationship between the pharmaceutical hydrochlorides dissolved in water and those bound on TMONPs. Ultimately, the method of standard additions may prove itself to be the most practical analytical approach towards accurate determination of PAC levels in environmental water especially when mass spectrometry detection is hyphenated with CE. After using TMONPs as adsorbents for the efficient removal of pharmaceuticals in environmental water source remediation, the feasibility of their regeneration under optimal desorption conditions must be fully demonstrated to keep investment costs down.

Data availability

The data sets supporting this article will be made available on request.

Author contributions

Conceptualization, Edward Lai; data curation, Eman Elmorsi; funding acquisition, Edward Lai; investigation, Eman Elmorsi; methodology: Eman Elmorsi and Edward Lai; project administration, Edward Lai; resources, Edward Lai; supervision, Edward Lai; writing – original draft, Eman Elmorsi; and writing – review & editing, Edward Lai.

Conflicts of interest

The authors declare no competing financial interest.

Acknowledgements

The authors acknowledge the Natural Sciences and Engineering Research Council of Canada (NSERC) RGPIN-2018-05320 for the financial support of this research.

References

1 M. R. Letsoalo, T. Sithole, S. Mufamadi, Z. Mazhandu, M. Sillanpaa, A. Kaushik and T. Mashifana, *J. Cleaner Prod.*, 2023, **387**, 135798.
2 O. Canlı, E. Oktem Olgun, B. Güzel and M. Kaplan, *Int. J. Environ. Anal. Chem.*, 2022, **104**, 1778–1804.
3 S. Sharma, V. Sharma, A. Mittal, D. K. Das, S. Sethi, S. Yadav, B. Vallamkonda and V. K. Vashistha, *Water Environ. Res.*, 2024, **96**(8), 11106.
4 R. A. de Jesus, G. C. de Assis, R. J. de Oliveira, J. A. S. Costa, C. M. P. da Silva, M. Bilal, H. M. N. Iqbal, L. F. R. Ferreira and R. T. Figueiredo, *Environ. Technol. Innovation*, 2021, **24**, 101851.
5 A. B. Sengul and E. Asmatulu, *Environ. Chem. Lett.*, 2020, **18**, 1659–1683.
6 N. Thakur, N. Thakur, A. Kumar, V. K. Thakur, S. Kalia, V. Arya, A. Kumar, S. Kumar and G. Z. Kyzas, *Sci. Total Environ.*, 2024, **914**, 169815.
7 K. K. Yadav, M. M. S. Cabral-Pinto, A. Gacem, A. M. Fallatah, B. Ravindran, S. Rezania, J. S. Algethami, L. Bashier Eltayeb, M. Abbas, T. Hassan Al-shareef, V. Vinayak, C. Truong Son, M. Awjan Alreshidi, J. Manuel Rodríguez-Díaz and R. Z. Homod, *Mater. Today Chem.*, 2024, **40**, 102226.
8 M. Mohadesi, M. Sanavi Fard and A. Shokri, *Int. J. Environ. Anal. Chem.*, 2022, **104**, 2571–2592.
9 C. R. Babu, A. V. Avani, T. S. Xavier, M. Tomy, S. Shaji and E. I. Anila, *J. Energy Storage*, 2024, **80**, 110382.
10 Q. Wang, G. Zhu, Q. Wang, W. Zhao, Y. Li, N. Shakoor, Z. Tan, F. Wang, P. Zhang and Y. Rui, *J. Environ. Manage.*, 2024, **368**, 122186.
11 S. Attarilar, J. Yang, M. Ebrahimi, Q. Wang, J. Liu, Y. Tang and J. Yang, *Front. Bioeng. Biotechnol.*, 2020, **8**, 822.
12 T. Atugoda, M. Vithanage, H. Wijesekara, N. Bolan, A. K. Sarmah, M. S. Bank, S. You and Y. S. Ok, *Environ. Int.*, 2021, **149**, 106367.
13 L. Wang, C. Shi, L. Wang, L. Pan, X. Zhang and J.-J. Zou, *Nanoscale*, 2020, **12**, 4790–4815.
14 P. R. Yaashikaa, P. S. Kumar, A. Saravanan and D.-V. N. Vo, *J. Hazard. Mater.*, 2021, **420**, 126596.
15 N. Dhiman and N. Sharma, *Environ. Technol. Innovation*, 2019, **15**, 100392.

16 T. M. Salem Attia, X. L. Hu and D. Q. Yin, *Chemosphere*, 2013, **93**, 2076–2085.
17 V. López-Ramón, C. Moreno-Castilla, J. Rivera-Utrilla and L. R. Radovic, *Carbon*, 2003, **41**, 2020–2022.
18 H. Gulley-Stahl, P. A. Hogan II, W. L. Schmidt, S. J. Wall, A. Buhrlage and H. A. Bullen, *Environ. Sci. Technol.*, 2010, **44**, 4116–4121.
19 T. X. Bui and H. Choi, *Chemosphere*, 2010, **80**, 681–686.
20 F. Claussen, J. Al-Gousous, N. Salehi, M. A. Garcia, G. L. Amidon and P. Langguth, *Pharm. Res.*, 2024, **41**, 937–945.
21 J. Gao and J. A. Pedersen, *Environ. Sci. Technol.*, 2005, **39**, 9509–9516.
22 F. L. Theiss, M. J. Sear-Hall, S. J. Palmer and R. L. Frost, *Desalin. Water Treat.*, 2012, **39**, 166–175.
23 S. M. Azcarate, L. Pinto and H. C. Goicoechea, *J. Chemom.*, 2020, **34**(12), e3246.
24 W. A. Jensen, *J. Qual. Technol.*, 2017, **49**, 186–188.
25 L. Vera Candioti, M. M. De Zan, M. S. Cámara and H. C. Goicoechea, *Talanta*, 2014, **124**, 123–138.
26 A. Morshedi and M. Akbarian, *Indian Journal of Fundamental and Applied Life Sciences*, 2014, **4**, 2434–2439.
27 K. Rajkumar and M. Muthukumar, *Appl. Water Sci.*, 2015, **7**, 637–652.
28 L. Yahia Cherif, I. Yahiaoui, F. Aissani-Benissad, K. Madi, N. Benmehdi, F. Fourcade and A. Amrane, *Ind. Eng. Chem. Res.*, 2014, **53**, 3813–3819.
29 M. Yousefi, R. Nabizadeh, M. Alimohammadi, A. A. Mohammadi and A. H. Mahvi, *MethodsX*, 2019, **6**, 35–42.
30 M. A. Watson, A. Tubić, J. Agbaba, J. Nikić, S. Maletić, J. Molnar Jazić and B. Dalmacija, *J. Hazard. Mater.*, 2016, **312**, 150–158.
31 P. Bangaraiah and B. Sarathbabu, *Chem. Eng. Commun.*, 2018, **206**, 986–993.
32 H. Alidadi, A. Ghorbanian, M. Ghorbanian, E. Rahmanzadeh, N. Nemanifar and M. Mehrabpour, *Desalin. Water Treat.*, 2018, **132**, 350–358.
33 M. Mourabet, A. El Rhilassi, H. El Boujaady, M. Bennani-Ziatni, R. El Hamri and A. Taitai, *Appl. Surf. Sci.*, 2012, **258**, 4402–4410.
34 C. Sarret, S. Barrière, G. Remerand, G. Massoullie, A. Chalard, C. Dauphin, B. Pontier and F. Laffargue, *J. Pediatr. Neurol.*, 2024, **22**(06), 425–428.
35 V. Muppavarapu, G. N. Challa, M. Gande, P. R. Billa, S. Gogineni and S. R. Yarraguntla, *Sep. Sci. plus*, 2024, **7**(8), e202400038.
36 A. Catalano, A. Carocci and M. Sinicropi, *Curr. Med. Chem.*, 2015, **22**, 1400–1413.
37 *CFR Part 439 – Pharmaceutical Manufacturing Point Source Category*, **https://www.ecfr.gov/current/title-40/chapter-I/subchapter-N/part-439**, accessed November 12, 2024.
38 K. Samal, S. Mahapatra and M. Hibzur Ali, *Energy Nexus*, 2022, **6**, 100076.
39 E. T. Elmorsi and E. P. C. Lai, *Int. J. Plant, Anim. Environ. Sci.*, 2024, **14**, 6–16.
40 E. T. Elmorsi and E. P. C. Lai, *Int. J. Plant, Anim. Environ. Sci.*, 2024, **14**, 6–16.
41 A. Flatie Alemu, A. Tegegne and N. Getaw, *Drug, Healthcare Patient Saf.*, 2024, **16**, 19–28.
42 F. Krebs, H. Zagst, M. Stein, R. Ratih, R. Minkner, M. Olabi, S. Hartung, C. Scheller, B. H. Lapizco-Encinas, C. Sänger-van de Griend, C. D. García and H. Wätzig, *Electrophoresis*, 2023, **44**, 1279–1341.
43 S. Krait, M. Konjaria and G. K. E. Scriba, *Electrophoresis*, 2021, **42**, 1709–1725.
44 W. A. Jensen, *J. Qual. Technol.*, 2017, **49**, 186–188.
45 A. Chabbi, M. A. Yallese, I. Meddour, M. Nouioua, T. Mabrouki and F. Girardin, *Measurement*, 2017, **95**, 99–115.
46 P. Szabová, D. Varjúová, M. Kováčová, J. Prousek and I. Bodík, *Pol. J. Environ. Stud.*, 2022, **31**, 1805–1812.
47 A. F. Pant, D. Özkasikci, S. Fürtauer and M. Reinelt, *Front. Chem.*, 2019, **7**, 00680.
48 N. Sivarajasekar, T. Paramasivam, R. Subashini, J. P. Maran and S. Kandasamy, *Asian J. Microbiol., Biotechnol. Environ. Sci.*, 2017, **19**, 130.
49 M. Bizi and F. E. El Bachra, *Molecules*, 2021, **26**, 7318.
50 Y. Bian, X. Chen and Z. J. Ren, *Environ. Sci. Technol.*, 2020, **54**, 9116–9123.